JOURNAL OF PROPULSION AND POWER
Vol. 22, No. 4, July–August 2006

Aerodynamic Performances of a Combined Cycle Inlet

Shinji Kubota*
Tohoku University, Miyagi 980-8579, Japan
Kouichiro Tani†
Japan Aerospace Exploration Agency, Miyagi 981-1525, Japan
and
Goro Masuya‡
Tohoku University, Miyagi 980-8579, Japan

Ramp-compression-type inlets for the combined cycle engine were investigated in a Mach 4 wind tunnel. Geometries of the inlet models were changed to investigate their effects on the aerodynamic performances and the starting characteristics. A bent cowl improved the starting characteristic by weakening the shock from the cowl leading edge to suppress the shock-induced separation and by reducing the internal contraction ratio of the cowl duct, thus, avoiding choking at the inlet throat. With the current geometries, the inlet started with a slightly larger internal contraction ratio than that restricted by the Kantrowitz–Donaldson limit. The ratio of the height of the cowl duct of the inlet to the incoming boundary layer was found to affect the starting characteristic. The model with a higher capture ratio showed better total pressure recovery performance.

Nomenclature

A	=	area
H	=	height of sidewall
h	=	height
M	=	Mach number
m_{cap}	=	mass capture ratio
P	=	pressure
w	=	width of inlet
x	=	distance from inlet entrance
α	=	sidewall sweptback angle
β	=	cowl lip angle to freestream
η_{KE}	=	kinetic energy efficiency
η_{Pt}	=	total pressure recovery
θ	=	ramp angle

Subscripts

c	=	cowl leading edge
in	=	entrance of inlet
out	=	exit of inlet
r	=	ramp
t	=	stagnation condition
w	=	wall
0	=	freestream condition

I. Introduction

ONE of the promising engines for a space plane is the combined cycle engine, which has the potential to maintain high specific impulse over a wide range of flight speeds by changing the operating cycles,[1] such as ejector jet, ramjet, scramjet, and rocket. One of the advantages of the combined cycle engine is that it can realize all of these operating cycles in a single flow passage so that the size and weight of the entire propulsion system can be reduced.

The inlet is an important part of the combined cycle engine because it compresses incoming air and provides it stably to the combustor. Its configuration must be optimized so that it can maintain high aerodynamic performances in different operating cycles.

There are several geometrical approaches for inlets of the combined cycle engine. Among them, the ramp-compression-type is favorable for the combined cycle engine because its simple geometry allows variable ramp and/or cowl configurations so that it can be adapted to various operation modes for specific speed ranges. It also enables closure of the entrance during reentry to the Earth's atmosphere.[2] With regard to practical designing, however, variable geometries would be constrained because of problems such as installation of cooling systems or mechanical complicacy. To avoid such problems, it is preferable to minimize the number of moving parts and to retain quasi-fixed geometries over a wide range of speeds. For that reason, it is important to clarify the effect of geometries on the performance.

The object of the present study was to investigate the effect of geometry on the aerodynamic characteristics of the ramp-compression-type inlets in the Mach 4 flow condition. In particular, around this Mach number, the inlet starting characteristic is an important issue because a more efficient ramjet mode is required instead of the ejector jet mode for a successful flight-path strategy.

In the current study, the length and angle of the cowl and the width of the entrance of the inlet were parametrically changed. The flowfield was observed by the schlieren method and wall pressure measurements. For each configuration, start/unstart conditions were experimentally determined based on the observation, and the effect of the geometrical parameters on the starting characteristic was investigated. The aerodynamic performances such as the mass capture ratio and total pressure recovery were also evaluated based on wall and pitot pressure measurements.

II. Experimental Apparatus and Models

The experiments were conducted in the 100×110 mm blowdown Mach 4 wind tunnel at the Japan Aerospace Exploration Agency, Kakuda. The freestream Mach number was 4.06 ± 0.005. The total pressure and total temperature of the freestream were 2.09 ± 0.03 MPa and room temperature, respectively. The unit Reynolds number was 1.1×10^8 m^{-1}. Figure 1 shows a schematic of the inlet model configuration. The inlet consisted of a cowl, a pair of sidewalls, a ramp block, and a top plate, the latter of which

Received 20 May 2005; revision received 29 August 2005; accepted for publication 19 November 2005.

*Graduate Student, Department of Aerospace Engineering, Sendai; currently Engineer, Turbine Design and Assembling Department, Toshiba Industry, Aoba-ku, Sendai, Miyagi 980-8578, Japan.

†Subgroup Leader, Engine System Subgroup, Combined Propulsion Research Group, 1 Kimigaya Koganezawa, Miyagi. Member AIAA.

‡Professor, Department of Aerospace Engineering, Aoba-ku, Sendai. Senior Member AIAA.

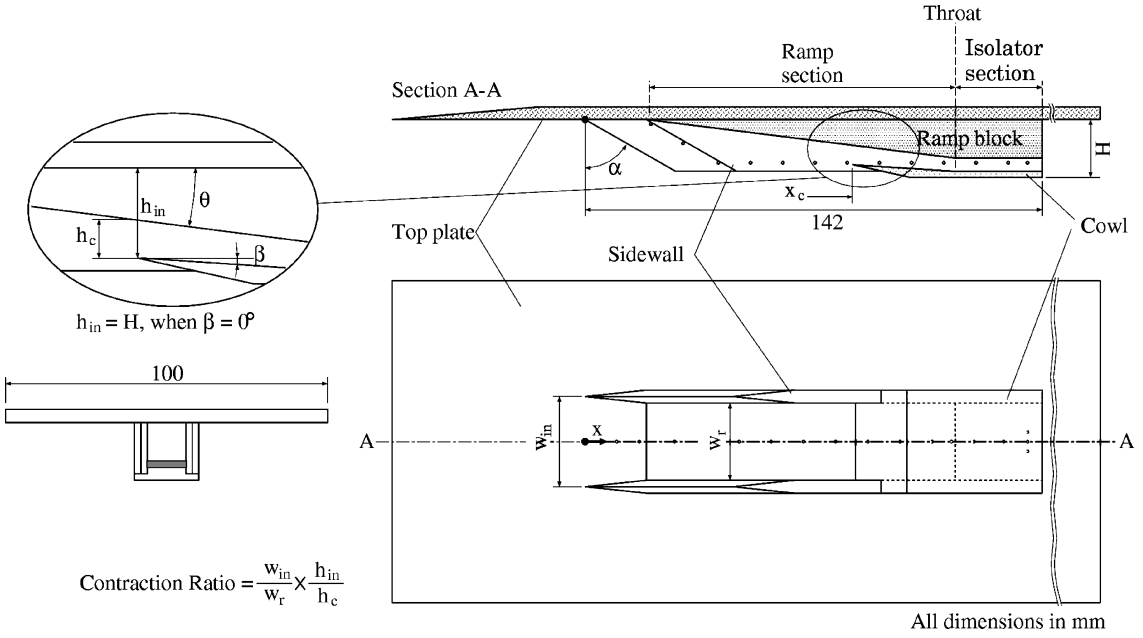

Fig. 1 Schematic of inlet model.

simulated the ventral surface of the vehicle. The overall length of the inlet was 142 mm and the height of the sidewall was 16.2 mm. The leading edge of the sidewall had a wedge shape with a 60-deg sweptback angle and a wedge length of 19.3 mm. Because of the shape of this wedge, a shock wave was generated and incoming air was compressed (side wall compression). The ramp, with a 7-deg compression angle, began just at the end of the sidewall wedge portion, and then the surface of the ramp ran parallel to the freestream direction at the throat.

The overall contraction ratio, $w_{\text{in}}/w_r \times H_{\text{in}}/H_c$, ranged from 4 to 5, depending on the geometry. The boundary layer, which developed on the top plate upstream of the model, was ingested into the model. Its 99% velocity thickness at the entrance of the inlet was 1.9 ± 0.1 mm according to the pitot pressure measurements.

A bent cowl was adopted to improve the starting characteristics of the inlet, with the aim of reducing the internal contraction of the cowl duct and weakening the cowl-originated shock wave, which induces boundary-layer separation. Here, the cowl duct corresponds to the part of the inlet where all four sides of the flow passage were solid walls (cowl, sidewalls, and top wall). The cowl was bent at the position where the ramp surface turns to parallel to the freestream direction, that is, the throat position.

The lesser number of engine modules reduces the mass of the sidewalls and also decreases the friction loss due to the smaller wet surface area. Therefore, the wider module is expected to increase overall performance of the entire propulsion system. To investigate the influence of the engine's cross-sectional aspect ratio, inlet models with three values of the width-to-height ratio, $w/H = 1$, 1.5, and 2, were examined. Because the horizontal contraction ratio changed in accordance with w/H, the height of the throat was adjusted so that the overall contraction ratio of the inlet was fixed at five for nonbending cowls.

Visualization by the schlieren method was adopted, and the outer flow around the inlet was observed. Pitot pressures at the inlet entrance and 5 mm upstream of the inlet exit were measured. The wall pressures along the top wall centerline, the cowl centerline, and the sidewall line with a height of 14.1 mm from the top plate were measured. The pressure was measured with a mechanical scanning device (Scanivalve®) with a 100-psi (700-kPa) range sensor. The data were then A/D converted and stored in a personal computer. End-to-end uncertainty of the pressure values was within 0.5%. Performances such as the starting characteristic, mass capture ratio, and total pressure recovery of the inlets were evaluated based on these measured values. Because of the uncetainty of the location of the probes and the pressure values, the mass flow and the averaged total pressure contained the error up to 8% and 10%, respectively.

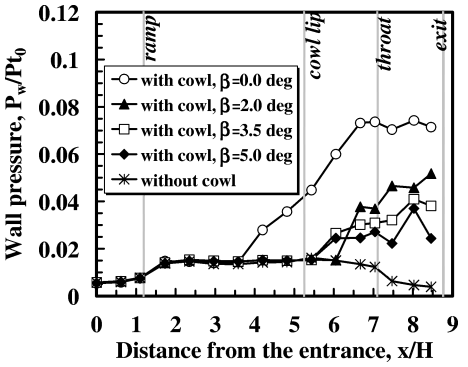

Fig. 2 Effect of bent cowl on wall pressure distributions on top wall: $w/H = 1.0$, $\alpha = 60$ deg, $\theta = 7$ deg, and $x_c/H = 5.25$.

III. Results and Discussion

A. Wall Pressure Distributions

Figure 2 shows the wall pressure distributions on the top wall of the inlet for the various cowl angles with a fixed cowl leading-edge position. The wall pressure P_w is normalized by the total pressure of the wind tunnel, P_{t0}, and the distance from the entrance, x, is normalized by the height of the sidewall, H. The pressure increased at $x/H = 1.7$ mainly due to a shock wave from the ramp corner. The location of the shock wave from the sidewall leading edge was estimated from the empirical equation proposed by Koide et al.,[3] and it was found that the two shocks from the sidewalls crossed around this region, $x/H = 1.52$, adding a small pressure rise. The crossing point moved to $x/H = 2.28$ and 3.04 in the case of $w/H = 1.5$ and 2.0, respectively. In the case of $\beta = 0$ deg, the wall pressure rose again upstream of the cowl lip, and a separation shock was observed by visualization. In the case of $\beta = 2$ deg, a second wall pressure rise occurred downstream of the cowl lip, and no separation shock was observed. With the larger β, the pressure always rose downstream of the cowl lip. The bent cowl showed the effect of relieving the pressure rise and the consequent separation formation.

B. Starting Characteristics

1. Categorization of Flowfield

As shown, the cowl created a high-pressure field in its downstream region in the cowl duct. Inlet unstart occurred in the following

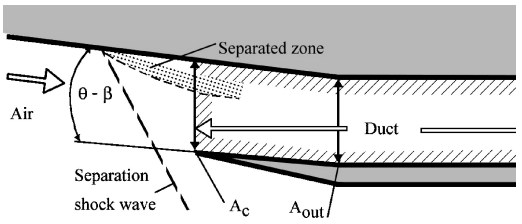

Fig. 3 Definition of inlet geometries and separation shock wave.

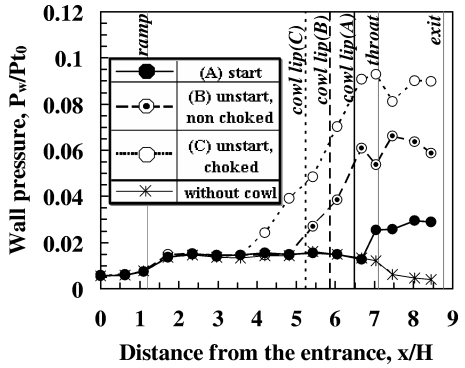

Fig. 4 Three flowfields, wall pressure distributions on top wall: $w/H = 1.0$, $\alpha = 60$ deg, $\theta = 7$ deg, and $\beta = 0$ deg.

two manners. One was that the flow was choked by the quasi-one-dimensional constraint. In this case, the strong shock wave was formed at the front of the cowl lip during the starting process of the wind tunnel. Once this shock wave was formed, it resided there even after the stable flow was established. The Kantrowitz–Donaldson (KD) condition (see Ref. 4) corresponds to this constraint. This condition describes the relation between the Mach number at the entrance of the internally converging duct and the in-and-out area ratio of the duct. In this relation, it is assumed that the flow, which first decelerates to subsonic speed by the normal shock wave attached at the entrance of the duct, is then accelerated and choked at the end of the duct. As for the current study, the critical internal contraction ratio of the cowl duct, A_c/A_{out}, was defined corresponding to the KD condition. Here, A_c is the area of the cross section at the cowl leading edge and A_{out} is the area at the exit of the inlet (Fig. 3).

The other case was that in which the large separation of the boundary layer, which occurred due to the large adverse pressure gradient, affected the internal flow structure. In this case, the size of the separation grew larger during the starting process of the wind tunnel as the flow speed rose. Once the separation shock wave traveled upstream of the cowl lip, the leakage became significantly greater, and the inlet fell to unstart. One parameter that influences the magnitude of the adverse pressure gradient is the internal contraction angle of the cowl duct, defined as $\theta-\beta$ (Fig. 3). With the larger internal contraction angle, shock waves that formed in the duct became stronger and caused the separation of the boundary layer on the ramp surface. This separation led to the formation of a separation shock wave upstream of the cowl lip that caused the additional spillage of the incoming air.

Here, the flow conditions in the inlet were categorized into the following three statuses (Fig. 6):

A. A separation shock wave was not formed upstream of the cowl leading edge (start).

B. A separation shock wave was formed upstream of the cowl leading edge. However, the flow was not choked upstream of the throat of inlet (unstart, nonchoked).

C. A separation shock wave was formed upstream of the cowl leading edge. Concurrently, the flow was choked around the throat of inlet (unstart, choked).

Figure 4 shows typical wall pressure distributions of these three flow statuses. The existence of a separation shock wave was detected from these wall pressure distributions and visualization by

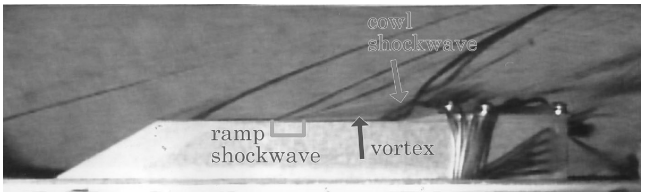

a)

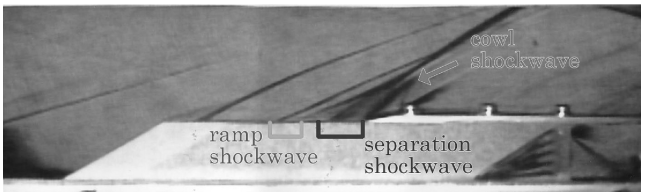

b)

Fig. 5 Schlieren photographs of two flowfields: a) start and b) unstart with separation shock.

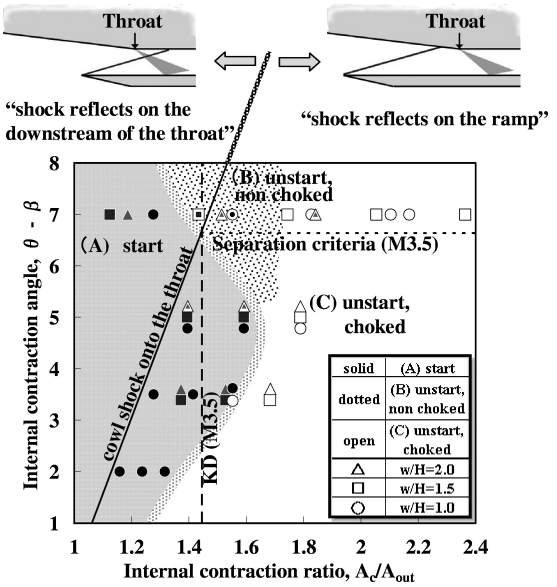

Fig. 6 Starting characteristics and inlet geometry.

the schlieren method, shown in Fig. 5. No significant difference could be observed in the top wall pressure distribution of conditions B and C. Only the throat conditions could determine their distinctiveness. In the current study, choking was determined so that the mass flow at the exit calculated from the pitot pressure reached a value that was more than 95% of the assumed choked mass flow, which was evaluated from the total temperature, the total pressure, and the cross-sectional area at the model exit.

Figure 6 shows the relationship between the geometry of the inlet and the starting limits. The horizontal axis refers to the internal contraction ratio A_c/A_{out}, and the vertical axis refers to the internal contraction angle $\theta-\beta$. Note that in the case where the data took the same coordinate, the marks plotted in Fig. 6 are slightly shifted in the vertical direction. There were four values of $\theta-\beta$, that is, 2, 3.5, 5, and 7 deg. The three flow conditions A∼C are shown with solid symbols (start), dotted symbols (unstart, nonchoked), and open symbols (unstart, choked), respectively. The region of Fig. 6 can be roughly divided into the three flow conditions.

2. *Effect of Internal Contraction Ratio*

In Fig. 6, the KD condition for Mach 3.5, that is, $A_c/A_{\text{out}} = 1.45$, is shown by a dashed line. In this case, the freestream of Mach 4.0 decelerated to that speed due to the ramp shock wave with a 7-deg deflection angle. Note that the effective KD condition limit becomes somewhat less than 1.45 due to the displacement by the boundary

layer. Most of the inlets with the internal contraction ratio below KD conditions started.

Van Wie et al. conducted an inlet experiment to investigate the major factors involved in the starting characteristics.[5] In the case where the ratio of the boundary layer to the height of the inlet was sufficiently small, they concluded that the starting contraction ratio could be predicted by the KD conditions, with an accuracy of roughly 10%. In the present study, the boundary of the starting limit was also located with an accuracy of 10% of the KD conditions.

3. Effect of Internal Contraction Angle

The solid line in Fig. 6 indicates the condition at which the cowl shock wave impinges on the throat. On the right side of the line, the cowl shock wave is reflected on the ramp. On the left side of the line, it is reflected on the downstream of the throat. In the case with $\theta-\beta=7$ deg, no inlets on the right side of the line started, whereas some on the left side of the line did. In the latter cases, the expansion wave from the throat corner suppressed the propagation of the boundary-layer separation from the ramp surface. On the other hand, some of the inlets started when $\theta-\beta$ was less than 5 deg, even when the cowl shock wave impinged on the ramp surface. The pressure rise on the ramp surface by the cowl shock wave becomes larger with the larger contraction angle, and, with a certain pressure rise, boundary-layer separation is inevitable. Several boundary-layer separation models have been proposed. For example, Mager[6] has proposed a model of shock-induced separation and formulated the relation between the Mach number and the critical pressure rise required for boundary-layer separation. This separation criterion was applied to the pressure rise on the ramp surface and is also shown in Fig. 6 by a dotted line. When the shock was reflected on the ramp, with a small internal contraction condition, this criterion roughly gave the limit of the start.

4. Effect of Cross-Sectional Aspect Ratio

In Fig. 6, the parameter of w/H is symbolized by circles, $w/H=1.0$; squares, $w/H=1.5$; and triangles, $w/H=2.0$. There is no significant difference with the difference of w/H, except in the case that $\theta-\beta=5$ deg and $A_c/A_{\text{out}}=1.4\sim1.6$. In this exceptional case, the inlets with $w/H=1$ and 1.5 started, but the inlet with $w/H=2.0$ did not. A test with a thinner incoming boundary layer was conducted by removing part of the top plate upstream of the inlet, and the inlet with $w/H=2.0$ finally started (Fig. 7). In the current configuration, as the w/H becomes larger, the height of the throat becomes smaller. This result suggests that the ratio of the duct height to the thickness of the boundary layer was one of the factors for the starting characteristic.

C. Inlet Aerodynamic Performances

1. Geometrical Effects

Figure 8 shows the mass capture ratio for all tested configurations. The mass capture ratio m_{cap} is plotted as a function of A_c/A_{in}, where A_{in} is the area of the cross section at the inlet entrance. The same symbols as those in Fig. 4 are employed.

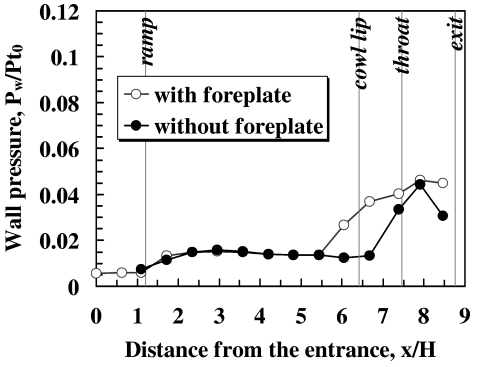

Fig. 7 Influence of thickness of boundary layer on wall pressure distributions on top wall: $w/H=2.0$, $\alpha=60$ deg, $\beta=2$ deg, and $\theta=7$ deg.

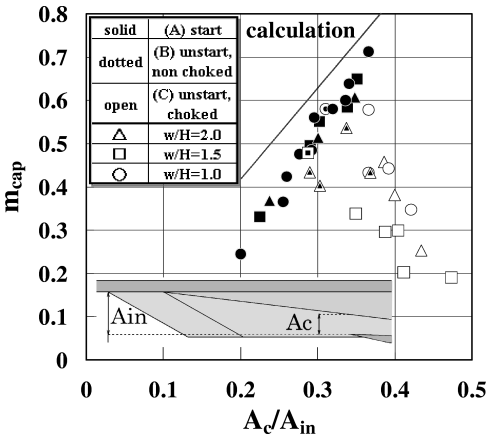

Fig. 8 Mass capture ratio and inlet geometry.

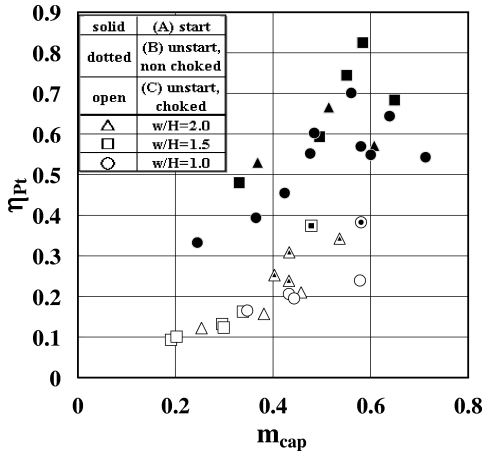

Fig. 9 Relation between total pressure recovery and mass capture ratio.

When it is assumed that a two-dimensional oblique shock wave emanated from the ramp corner, the streamline attached to the cowl lip could be estimated, and the mass capture ratio could be defined as the ratio of the height of this streamline at the entrance to the overall inlet height. The result of this calculation is also shown in Fig. 8 by a solid line.

The captured mass flow rate m_{cap} changed linearly to A_c/A_{in} as long as the inlet started. Although it gave a slightly greater value, the calculation estimated the gradient factor of m_{cap} to A_c/A_{in} well. The comparison indicated that most of the spillage was created by the ramp shock.

When the inlet was in the unstart condition without choking, m_{cap} had a greater value with an increment of A_c/A_{in}. In the current definition, the increment of A_c/A_{in} corresponded to two situations. One was that β became smaller, and the other was that the cowl lip was located farther upstream. Although there was a separation shock that produced additional spillage, this tendency revealed that the amount of the flow scooped by the longer cowl increased to some extent.

In the case of unstart with choking, as A_c/A_{in} increased m_{cap} decreased. In this case, the separation shock wave shifted farther upstream and drastically increased the spillage of the main stream, which had a high total pressure, thus, resulting in a decrease of the total pressure at the exit of the inlet. In the choked flowfield, lower total pressure led to a decrease of m_{cap} for the constant area and a decrease of total temperature.

Figure 9 shows the total pressure recovery η_{Pt} for all tested configurations, where η_{Pt} is the ratio between the mass-averaged total pressure at the entrance and the exit of the inlet. Here, η_{Pt} is plotted as a function of m_{cap}. In the started condition, η_{Pt} increased as the m_{cap} increased. When m_{cap} increased, in general, the compression

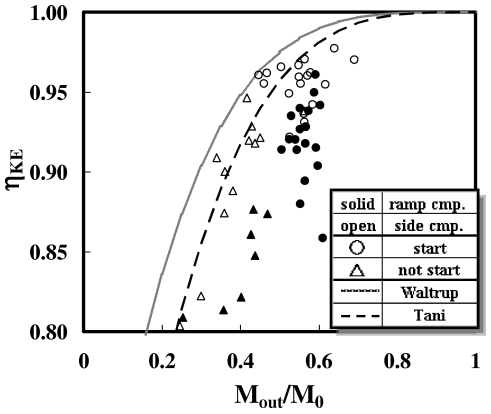

Fig. 10 Comparison of efficiencies between ramp compression inlet and sidewall compression inlet.

ratio became larger, and, thus, the total pressure loss by the shock waves became larger. On the other hand, the increase of m_{cap} meant that the ratio of mass flow of the boundary layer, which had the lower total pressure, to the entire captured mass decreased. This result indicated that the latter effect was more dominant in the current geometry. In the choked condition η_{Pt} increased linearly to m_{cap}, the reason being that the choked mass flow is proportional to the total pressure with constant total temperature and constant area. In the case of unstart with nonchoking, η_{Pt} was distributed between the values of the start and the unstart with choking, and it also tended to increased as m_{cap} increased.

2. Comparison with Side Wall Compression-Type Inlets

Tani et al.[7,8] tested the sidewall compression-type inlet with almost the same scaled geometries as those of the present study to examine the geometrical effects on the starting characteristic. Figure 10 shows a comparison of the kinetic energy efficiency η_{KE} between the ramp compression inlet and the sidewall compression inlet. In Fig. 10, η_{KE} is plotted as a function of the exit to freestream Mach number ratio M_{out}/M_0. The result of the ramp compression inlet and the sidewall compression inlet are plotted with solid symbols and open symbols, respectively. Because the trichotomous classification introduced earlier cannot be applied to the status of the flowfield in the sidewall compression inlet, dichotomous categorization (start/unstart) is adopted here, based on the existence of a separation shock upstream of the cowl lip. The conditions are shown by circles (start) and triangles (unstart). Note that the values were normalized by the free stream quantities instead of the averaged ones at the inlet entrance. The empirical estimations by Waltrup et al.[9] and Tani et al.[8] are also shown by solid and dashed lines, respectively.

In general, the sidewall compression inlet showed a better performance than the ramp compression inlet. One of the reasons for the lower performance of the ramp inlet was the difference of the point where pitot pressures were measured. For the sidewall compression inlet, the data were obtained at the end of convergent section (cowl leading-edge location), whereas they were captured at the exit of the model for the ramp inlet. Thus, the values of the ramp inlet were affected by the shock waves in the cowl duct.

IV. Conclusions

The ramp-compression-type inlets of the combined cycle engine were experimentally investigated in Mach 4 flow conditions. The model geometries were changed parametrically, and the following points were clarified:

1) The flowfield in the ramp-compression-type inlet was categorized into three conditions, that is, start, unstart without choking, and unstart with choking.

2) The bent cowl improved the starting limit of the inlet.

3) The maximum internal contraction ratios at which the inlets started were around the KD limits.

4) The smaller ratio of the height of the duct section to the thickness of the incoming boundary layer led to the unstart of the inlet.

5) In the case of the start, the loss of the total pressure by spilling of the main stream, which has a high total pressure, was greater than that by the shock wave formed in the inlet. Thus, the total pressure recovery became greater with the higher capture ratio.

6) The smaller internal contraction angle improved the starting characteristic. The point of shock impingement on the ramp surface was found to be one of the elements affecting the starting characteristic.

Acknowledgments

The authors acknowledge Takeshi Kanda of the Japan Aerospace Exploration Agency (JAXA) for useful advice and Kenji Kudo and Kanenori Kato of JAXA for their tremendous help in conducting the experiments.

References

[1]Russell, D., and Corin, S., "Combined Rocket and Airbreathing Propulsion Systems for Space-Launch Applications," *Journal of Propulsion and Power*, Vol. 14, No. 5, 1998, pp. 605–612.

[2]Kanda, T., and Kudo, K., "Cooling Requirement of the Combined Cycle Engine in Descending Flight," *Proceedings of 24th International Symposium on Space Technology and Science*, Japan Society for Aeronautical and Space Sciences and Organized Committee of 24th ISTS, Tokyo, 2004, pp. 39–44.

[3]Koide, S, Griesel, C. J. W., and Stollery, J. L., "Correlation of Shock Angles Caused by Rhombic Delta Wing," *AIAA Journal*, Vol. 34, No. 9, 1996, pp. 1958–1960.

[4]Crocco, L., "One-Dimensional Treatment of Steady Gas Dynamics," *Fundamentals of Gas Dynamics*, 2nd ed., edited by H. W. Emmons, Princeton Univ. Press. Princeton, NJ, 1967, pp. 184–190.

[5]Van Wie, D. M., Kwok, F. T., and Walsh, R. F., "Starting Characteristics of Supersonic Inlet," AIAA Paper 96-2914, July 1996.

[6]Mager, A., "On the Model of the Free, Shock-Separated, Turbulent Boundary Layer," *Journal of the Aeronautical Sciences*, Vol. 23, Feb. 1956, pp. 182–184.

[7]Tani, K., Kanda, T., and Tokunaga, T., "Starting Characteristics of Scramjet Inlets," *Proceedings of 11th ISABE*, 1993, pp. 1071–1080.

[8]Tani, K., Kanda, T., Kudo, K., Murakami, A., Komuro, T., and Itoh, K., "Aerodynamics Performance of Scramjet Inlet Models with a Single Strut," AIAA Paper 93-0741, Jan. 1993.

[9]Waltrup, P. J., Billig, F. S., and Stockbridge, D., "Engine Sizing and Integration Requirements for Hypersonic Airbreathing Missile Applications," CP-307, AGARD, March 1982.